Methods 115 (2017) 128–143

Contents lists available at ScienceDirect

Methods

journal homepage: www.elsevier.com/locate/ymeth

Ultrasound registration: A review

Chengqian Che [a], Tejas Sudharshan Mathai [b], John Galeotti [a,b,*]

[a] Department of Biomedical Engineering, Carnegie Mellon University, 5000 Forbes Ave, Pittsburgh, PA 15213, USA
[b] The Robotics Institute, Carnegie Mellon University, 5000 Forbes Ave, Pittsburgh, PA 15213, USA

ARTICLE INFO

Article history:
Received 16 July 2016
Received in revised form 7 December 2016
Accepted 8 December 2016
Available online 11 December 2016

Keywords:
Registration
Ultrasound
IMAGE analysis algorithms and methods
Volume reconstruction
Image alignment
Matching
Warping
Transforms
Metrics
Optimization
Rigid
Non-rigid
Matrix
Elastic
Inelastic
2D
3D

ABSTRACT

This article is a review of registration algorithms for use between ultrasound images (monomodal image-based ultrasound registration). Ultrasound is safe, inexpensive, and real-time, providing many advantages for clinical and scientific use on both humans and animals, but ultrasound images are also notoriously noisy and subject to several unique artifacts/distortions. This paper introduces the topic and unique aspects of ultrasound-to-ultrasound image registration, providing a broad introduction and summary of the literature and the field. Both theoretical and practical aspects are introduced. The first half of the paper is theoretical, organized according to the basic components of a registration framework, namely preprocessing, image-similarity metrics, optimizers, etc. It further subdivides these methods between those suitable for elastic (non-rigid) vs. inelastic (matrix) transforms. The second half of the paper is organized by anatomy and is practical in nature, presenting and discussing the complete published systems that have been validated for registration in specific anatomic regions.

Contents

1. Introduction . . . 129
2. Pre-processing . . . 130
   2.1. Noise removal . . . 130
   2.2. Multi-resolution and down-sampling . . . 130
   2.3. Image segmentation and feature detection . . . 130
3. Registration metrics . . . 131
   3.1. Well established similarity metrics used in both rigid and non-rigid registration . . . 131
   3.2. Well established feature-based metrics . . . 131
   3.3. Similarity metrics used only in rigid registration . . . 132
      3.3.1. Novel . . . 132
      3.3.2. Adapted . . . 132
   3.4. Similarity metrics used only in non-rigid registration . . . 132
      3.4.1. Novel . . . 132
      3.4.2. Adapted . . . 132
4. Registration optimizers . . . 132

* Corresponding author at: Robotics Institute, Carnegie Mellon University, 5000 Forbes Ave, Pittsburgh, PA 15213, USA.
E-mail addresses: cche@andrew.cmu.edu (C. Che), tmathai@andrew.cmu.edu (T.S. Mathai), jgaleotti@cmu.edu (J. Galeotti).

http://dx.doi.org/10.1016/j.ymeth.2016.12.006
1046-2023/

4.1. Optimizers used only in rigid registration . . . 133
4.1.1. Adapted . . . 133
4.2. Optimizers used only in non-rigid registration . . . 133
4.2.1. Novel . . . 133
4.2.2. Adapted . . . 133
5. Registration techniques and results by anatomy . . . 134
5.1. Head . . . 134
5.2. Neck . . . 136
5.3. Breast . . . 136
5.4. Heart . . . 136
5.5. Liver . . . 137
5.6. Kidney . . . 137
5.7. Gall bladder . . . 137
5.8. Bone . . . 138
5.9. Prostate . . . 138
5.10. Fetal imaging . . . 138
6. Discussion, Shortcomings, and future opportunities . . . 139
6.1. Diverse anatomy and ultrasound systems . . . 140
6.2. Interactive nature of ultrasound acquisition . . . 140
6.2.1. Physical probe tracking . . . 140
6.2.2. Viewpoint specific . . . 140
6.2.3. Interactive manipulation during ultrasound acquisition . . . 140
Acknowledgements . . . 141
References . . . 141

1. Introduction

This article is a review of registration algorithms for use between ultrasound images (monomodal registration). We review the algorithms that have been published during the years 1998–2016 to address rigid and non-rigid registration of ultrasound-to-ultrasound only. Ultrasound imaging is a non-invasive, real-time, and lower cost alternative to other medical imaging modalities, providing many advantages for clinical and scientific use on both humans and animals. Ultrasound does not expose the patient to ionizing radiation, provides continuous real-time video imaging, and is generally painless. Ultrasound imaging has been used in various fields of medicine such as imaging the human brain, heart, liver etc. [1–3], and ultrasound is increasingly being used in animal studies, including, e.g., porcine brain [4], porcine carotid artery [5], and mice [6]. In many cases, multiple ultrasound images or volumes are acquired by either free-hand scans of the anatomical region of interest, or following a specific pattern of scanning through the rotation and translation of the ultrasound transducer. Regardless of scan pattern, the transducer is usually pushed into the region of interest to obtain better signal-to-noise ratio (SNR), deforming tissue in the process.

As ultrasound imaging produces a continual stream of images (or volumes), it is often necessary to register these images together, either for clinical evaluation of the entire organ, or to be used intra-operatively [7]. Unfortunately, ultrasound images are also notoriously noisy and subject to several unique artifacts/distortions. *Unlike multimodal registration (which typically benefits from higher-quality CT or MRI images against which to register the ultrasound images), monomodal ultrasound image-based registration algorithms bring two ultrasound images into alignment with one another based solely on the ultrasound data.*

Monomodal ultrasound registration, though challenging, is important for a growing body of work. For longitudinal studies, ultrasound imaging avoids accumulating MRI cost, CT radiation, and exposure to potentially harmful MRI-or-CT contrast agents. Diagnosis may require searching for meaningful differences between ultrasound images that were acquired months or years apart. Population studies compare ultrasound images between large numbers of subjects, often to disambiguate normal vs. pathological variation. Finally, it is desirable to combine multiple 2D ultrasound slices in a single 3D dataset, either when 3D ultrasound transducers are not an option, or when 2D transducers produce higher quality images.

Sometimes, the 3D spatial location and orientation of the ultrasound probe is also known through the use of ultrasound probe trackers [7,8]. However, probe tracking is also subject to error, especially for lower-accuracy electromagnetic (EM) trackers. Furthermore, probe tracking results in structural misalignment due to soft-tissue deformation, which is not directly measurable by probe tracking. For both reasons, image-based registration is still usually required to refine the tracker's initial registration estimate.

A registration process should result in the transform that best (however defined) aligns an image that needs to be registered (generally called the moving image) to a reference or fixed image. Registration transforms are typically grouped into two major classes: Rigid (or matrix) transformations and non-rigid (elastic) transformations. Within these classes, each transformation type has certain characteristic degrees of freedom (DOF). Degrees of freedom represent the number of independent parameters that are necessary to specify a transform, such as rotations and translations. Matrix transforms are generally of four types: strictly rigid, similarity, affine, and perspective. All these matrix transforms can perform rotations and translations. Similarity transforms can also perform scaling, and affine transforms can perform all of this plus shearing. Perspective transforms (which do not require parallel lines to remain parallel) are the most free-form matrix transform. These degrees of freedom for these matrix transforms, listed below in Table 1, constrain the warp of the moving image onto the fixed image. Closely related to matrix transforms are Quaternions, which are also a strictly rigid transform, but use a special representation so-as to avoid singularities in 3D rotation. Non-rigid transforms can have many more DOFs (e.g., vector fields

Table 1
Degrees of freedom (DOF) for matrix transforms.

Dimensionality	Strictly rigid	Similarity	Affine	Perspective
2D	3	4	6	8
3D	6	7	12	15

can have thousands), and can thus model elastic deformations of anatomical objects. With so many DOFs, non-rigid transforms typically require regularization in order to maintain spatial order and regularity. Other terms for non-rigid include deformable and elastic. There are two common situations in ultrasound image registration for which a rigid-body or matrix transformation would be used. The first situation is registration of non-deformable or inelastic anatomical structures such as bone. The second situation is as a simple (and quick) approximation when changes are small, often for deeper organs such as liver or else to initialize a subsequent deformable registration. On the other hand, non-rigid transforms, such as a B-spline or Thin Plate Spine deformation, are frequently used in ultrasound image registration due to the deformable nature of soft tissue such as organs, vessels, or the brain.

The rest of the paper is organized as follows: in the pre-processing section, we elaborate the techniques employed for noise reduction, as well as image segmentation and feature detection approaches to guide rigid and non-rigid ultrasound registration. Next we describe the common registration metrics used in literature, and then we explain the different registration optimizers preferred by researchers over the years for rigid and non-rigid registration. We then detail complete registration methods specifically designed for different anatomical regions of the human body, and finally we summarize with a discussion of the methods used. This review paper is not an exhaustive review of the various registration algorithms proposed over the years that could potentially be applied to ultrasound. However, it serves to inform the reader of the different approaches that have been popularly used and validated for rigid and non-rigid ultrasound-to-ultrasound registration.

2. Pre-processing

Ultrasound images typically have substantial noise, shadowing, etc., making registration and analysis more difficult than for MRI or CT. Multiple image pre-processing algorithms have been applied on ultrasound images to aid registration. One common pre-processing technique is to apply noise removal filters (including interpolation techniques). Some registration algorithms incorporate image segmentation and/or feature extraction to guide the registration. These registration implementations are executed either on noise reduced ultrasound images or directly on raw ultrasound images. Also, if images' intensities are scaled differently, the image intensities can be adjusted in pre-processing, or else an additional intensity scaling parameter may be included in the registration model [9]. Below are methods used in the literature specifically for ultrasound-to-ultrasound registration. There are many other preprocessing methods that may also be useful, such as histogram equalization (intensity normalization) or bi-linear filtering (edge preserving smoothing).

2.1. Noise removal

One of the most common types of noise in ultrasound images is speckle noise, which is caused by the interference of coherent ultrasound waves scattered by tissue within each resolution cell (e.g., interference inside a single pixel) [10]. Although speckle can be used as a feature (speckle-based registration is discussed in Section 2.3), speckle degrades the quality of ultrasound images and can lead to poor registration if neither suppressed nor explicitly utilized. Researchers have applied different noise-removal techniques before registration. One technique is to apply Gaussian filtering [3–10] to reduce the speckle noise in the image by blurring. More significantly, certain characteristics of an image, such as edges and ridges, can be preserved and enhanced by applying a bank of filters including Gaussian smoothing filter, the first derivative filter (gradient operator), the second derivative filter, the Laplacian filter, and threshold operators [11]. Oscillatory functions were used to reduce noise in [17]. Another common filter to reduce noise, especially speckle noise, is median filtering [18–22]. A median filter works as a non-linear low-pass filter, assigning to each pixel the median of its local (2D or 3D) neighboring values. Median filtering can potentially preserve image details while suppressing noise better than blurring, since the median is robust against outliers [20]. In [20], the S-Mean filter was proposed to more effectively remove speckle noise. This filter performs anisotropic diffusion to reduce speckle (SRAD) followed by a median filter. SRAD itself was introduced in [23] to preserve and enhance prominent edges. When used with anisotropic diffusion, the median filter was shown to reduce speckle noise with minimal edge degradation.

2.2. Multi-resolution and down-sampling

Multi-resolution (e.g. coarse-to-fine) approaches are common in image optimization tasks. Compared to "regular" (single-resolution) ultrasound registration algorithms, using a multi-resolution strategy usually has a higher convergence radius, is more robust to poor local optima, and progresses faster. Image pyramids are used to down sample both the fixed and moving images to a variety of scales, registering first on coarse, low-resolution images and then progressively refining that registration at increasing resolutions. In [12,15,24–27], authors used multi-resolution strategies with specific down-sampling ratios to get better registration results.

2.3. Image segmentation and feature detection

Many registration algorithms incorporate image segmentation and feature extraction methods in order to guide the registration. Segmentation approaches identify "foreground" regions of interest (ROI) in the ultrasound images, optimizing the registration primarily for those specific regions while the "background" regions are either ignored or else registered in a somewhat under-constrained fashion. Automatic feature detection utilizes points of interest in the image, along with their local neighborhoods, as key points for registration.

One example of registration based on coarse segmentation used structural information about the interface between bone and soft tissue. Their algorithm starts by segmenting the image using Otsu's thresholding method [28] to obtain a good initial, approximate segmentation of the separation between the echogenic zone and the shadow zone. Next, a Sobel filter is applied to detect the horizontal bone interface, followed by averaging to remove noise. Then, a fusion of the output of Otsu's method and the detected horizontal bone interface is performed. This fused result is dilated to produce the final segmented regions of interest with structural information [22]. An interactive live-wire segmentation algorithm was featured in [17] where the user selected seed points on breast and kidney ultrasound images in order to extract structural outlines of specific objects in the images. The cost functions for live-wire algorithm included the gradient magnitude, gradient direction, Canny edge features [29] and Laplacian zero crossing features. In [30], the local phase information of an image was extracted first, and then it was segmented to obtain the boundaries of objects with smooth borders in the images. The approach published in [5] segmented the lumen and media-adventitial boundaries using the B-snakes algorithm published in [31]. In [32], a fully automated segmentation algorithm based on a Generalized Hough Transform (GHT) and subsequent model adaptation with increasing degrees of freedom was used to segment volumes

of the heart of babies, and obtain a deformable model of the aortic root in a pediatric patient. In [33], both the Endocardium at end-diastole and the Epicardium were manually segmented.

Feature extraction can also be used to improve the accuracy of ultrasound image/volume registration. Researchers extract edges and texture features in ultrasound volumes to improve the smoothness of their metric functions, which leads to better optimization and results [34]. They model speckle noise as an irregular and complex texture pattern in ultrasound images, leading them to employ a Gabor filter bank to analyze textures. Their corresponding metric function is more stable at large scales, and useful information such as edges are well preserved [4]. In [17,35–37], SIFT features [38] were detected and extracted from the ultrasound images, and then utilized for matching of the ultrasound images. In [39,40], corner features were detected based on the principal curvature values of the Hessian matrices obtained for every pixel in the ultrasound image.

One special feature used for ultrasound registration is speckle noise. Speckle results from random back-scattering in a resolution cell of the ultrasound beam, and its intensity distribution is proven to be non-Gaussian. A fully formed speckle is known to have a Rayleigh distribution in the envelope detected image and Fish-Tippet distribution in the log-compressed image [41]. Speckles as special features can be extracted and used for ultrasound registration, especially when misalignment is either minimal or else almost entirely translation. [41–44]. For instance, in [41], a feature detector is employed based on statistical theoretical distributions of fully formed speckle in an ultrasound image to generate edge maps. They demonstrated their method to accurately register ultrasound images with speckled data and to be more robust to noise than standard gradient-based methods.

3. Registration metrics

A registration *metric* quantifies the similarity between two corresponding images based on a postulated transform between them. The metric, also known as a *similarity measure*, is used by the registration optimizer to solve for a transform (matrix and/or displacement field) that puts the two images into alignment. A robust metric will reach either its largest or smallest possible value when the two images are in alignment, and would ideally monotonically fall away for non-perfect alignments. Generally, registration metrics can be used to establish similarity between 2D images, 3D volumes, or even 4D/5D hyper-volumes. Pixel (or voxel)-based metrics have been developed and implemented widely in ultrasound registration. Pixel-based metrics compare the images' overlapping pixel values [13], as opposed to other metrics which compare non-pixel values (such as extracted features). Over the past few decades, a great number of similarity metrics have been proposed and developed in the medical imaging and computer vision communities. There is not yet a solid theoretical basis for choosing one similarity metric over another, and any given metric's performance depends significantly on other registration factors, including (1) the optimizer and its parameters, (2) the anatomical structures being imaged, (3) the dimensionality of the registered object, (4) the nature of the transformation (rigid/Quaternion, affine, non-rigid flow, non-rigid finite elements, etc.). Table 2 lists a variety of similarity metrics that have been used for ultrasound registration.

3.1. Well established similarity metrics used in both rigid and non-rigid registration

Mutual Information (MI) is a popular image similarity metric for both rigid and non-rigid medical image registration. Mutual information was initially introduced as a similarity metric by [45] and [46]. This metric seeks a transform that aligns two (ultrasound) images or volumes by maximizing their mutual information. The metric measures how much information one variable (image or volume) contains about the other. As [45] proposed, both the joint entropy and the individual entropies are used to obtain the mutual information. MI will be optimal when the individual entropies are maximized while joint entropies are minimized. MI is robust to outliers, and it is efficient to use in optimization, making MI an excellent metric [19,21,24,46,47–52].

Table 2
Similarity metrics used for ultrasound registration.

Registration type		Similarity metric
Standard Pixel-Based Metrics, Well Validated for both Rigid and Non-Rigid Transforms:		Mutual Information (MI), Normalized Cross Correlation (NCC), Correlation Coefficient (CC), Sum of Squared Differences (SSD)
Standard Feature-Based Metrics for both Rigid and Non-Rigid Transforms:		Manual Key Points, Automatic SIFT Feature Detection, Speckle Utilization, Application of pixel-based methods locally around key points
Unique Metrics, Rigid Validation Only	Novel Metrics:	Hellinger Distance + statistics-based Fuzzy Local Binary Patterns (FLBP), N-dimensional Mutual Information Matrix
	Adapted Metrics:	Correlation Ratio (CR), Sum of Absolute Differences (SAD)
Unique Metrics, Non-Rigid Validation Only	Novel Metrics:	SSD of pixel intensities + weighted SSD of local phase information, similarity metric $Sim(s_1, s_2)$ based on comparing attribute vectors
	Adapted Metrics:	SIFT matching, sample variance

Normalized Cross-Correlation (NCC) is another widely used similarity metric. NCC calculates the correlation between two functions, and it is considered to work the best with mono-modality registration between two images acquired with the same characteristic curves (e.g., same gamma curve). The NCC metric has been incorporated in both rigid [22] and non-rigid registration algorithms [53,27] with good results.

Correlation Coefficient (CC) is another prevalent similarity measure in literature. CC measures the linear correlation between two variables, outputting a degree of correlation between 0 and 1. It is simpler than NCC, but can be less robust to variations in imaging parameters (slightly different characteristic curves, etc.). CC can still perform well when used as a similarity metric in ultrasound registration with rigid transformation [13] and non-rigid transformation [54].

Sum of Squared Differences (SSD) is perhaps the simplest standard similarity metric in image registration. This metric calculates the sum of squared differences of pixels' or voxels' intensity from both reference and moving images or volumes. As this metric requires both reference and moving images/volumes to have the same intensity range, SSD is best-suited for mono-modality ultrasound registration. SSD for rigid [55], and non-rigid [5,25,33,56–63] registration has been discussed in recent papers.

3.2. Well established feature-based metrics

Feature Key Points were extracted using a wide variety of methods in [17,35–37,39,40], and the local neighborhoods around these keypoints were used in order to match them together prior to registration. The combination of feature detection and localized pixel intensity matching was a key component for the registration algorithms used in these papers. Identification of other features such as SIFT and Speckle was previously discussed in the preprocessing section. Once features have been identified, they can be mapped across images to create various metrics.

3.3. Similarity metrics used only in rigid registration

3.3.1. Novel

A novel hybrid procedure for rigid registration was proposed in [64]. The novel similarity metric is based on Hellinger distance between the distributions in images on the global scale, and a statistics-based extension of Fuzzy Local Binary Patterns (FLBP) on a local scale. Many methods are proposed to measure the similarity between LBPs, and histogram intersection is considered to be the most common one. Since histogram intersection may yield local minima, the Hellinger distance is preferred, which measures the statistical similarity of two distributions. Statistical similarity is globally precise but is locally imprecise. In contrast, the statistics-based FLBP is globally imprecise and locally precise. Thus, the combination of both components is desirable to achieve a large convergence radius (global) and a precise final result (local).

Instead of using regular mutual information as similarity metric, [18] introduced a high-dimensional mutual information matrix obtained by calculating its eigenvalues. During registration, when two images are geometrically aligned, N-dimensional MI reaches its maximum 1. This non-negative metric can be extended to higher dimensions so that multiple images can be registered. It was shown to register multiple ultrasound images through simulation.

3.3.2. Adapted

Correlation Ratio (CR) is another metric derived from Cross correlation. CR was proposed in [13], and measures the functional dependence between two variables. CR has been shown to be suitable for mono-modality ultrasound rigid registration [12,34].

Another similarity metric that has been used in rigid registration is the Sum of Absolute Differences (SAD). SAD is similar to SSD, but SAD does not quadratically emphasize the pixels with the largest intensity differences. SAD was utilized in [12].

3.4. Similarity metrics used only in non-rigid registration

3.4.1. Novel

A novel similarity measure was proposed for deformable registration of ultrasound images in [65]. It is a modification of the HAMMER algorithm, which was originally proposed in [66] for elastic registration of brain MR images. This similarity metric uses an attribute vector, consisting of geometric-moment invariants that are defined on each voxel in a 3D image. The similarity measure of two voxels is obtained by comparing their attribute vector and it is defined as:

$$Sim(s_1, s_2) = \prod_i (1 - |av_i(s_1) - av_i(s_2)|)^{w_i}$$

where av_i is the i th element of the attribute vector. $Sim(s_1, s_2)$ is 1 for similar voxels and zero for dissimilar voxels [9].

The similarity metric was elaborated in [30] as a *compatibility coefficient* between two feature points present in the local phase of two ultrasound images:

$$r_{p_i q_i} = \alpha \cdot \beta \cdot \gamma$$

Here, p_i and q_i are the set of feature points extracted from the local phase information of each of the two ultrasound images. They also defined $N_a^{p_i}$ and $N_b^{q_i}$ with $a = 1, 2 \ldots .A; b = 1, 2 \ldots .B$ to be the points adjacent to the detected feature points. Thus, $\alpha(p_i, N_a^{p_i}; q_i, N_b^{q_i})$ is the disparity in Euclidean distance between feature points p and q_i, while $\beta(p_i, N_a^{p_i}; q_i, N_b^{q_i})$ is the disparity in the angle between the feature points. $\gamma(p_i, N_a^{p_i})$ is the spatial smoothness measured by the distance between p_i and $N_a^{p_i}$.

The similarity metric was defined in [6] as the sum of two parts: the SSD between the pixel intensities of the source and target image, and the weighted SSD of the local phase information of the source and target image. They worked on in vivo cardiac ultrasound images.

3.4.2. Adapted

In [67], the voxel intensity-based similarity metric proposed in [68,69] was used. Here the reference volume is not selected, so the similarity measure is the sample variance of a population, which represents the difference from the current mean intensity $\bar{x}$ for each voxel x in volume. The similarity metric proposed in [65] was adopted by [8,9,50,55].

4. Registration optimizers

An optimizer plays an essential role in an image registration framework. The goal of an optimizer is to search for the transformation that produces the best alignment of a moving image or volume with a reference image or volume. This is usually done through the maximization of a similarity metric (metrics are detailed in Section 3). *With ultrasound, a similarity metric will typically not be robust enough to determine the best transformation between the reference and moving images or volumes.* This is because speckle noise, along soft tissue deformation, affects the ultrasound data, and therefore contributes to the degradation in the similarity between two corresponding pixels or voxels. To mitigate these effects, a cost function is normally used in registration of ultrasound volumes. *The cost function will typically consist of a data term that represents the similarity measurement between two voxels, and a regularization term that penalizes unlikely deformations (especially in non-rigid registration).* An optimizer will aim to reach its optimal goal of correctly aligning and registering two images or volumes with minimal deformation and maximum similarity. Two desirable properties of an optimizer are its robustness and short convergence time. Therefore, a good ultrasound registration framework will incorporate the best optimizer and metric for registration of images or volumes. Mathematically, the cost function J to be minimized is defined as:

$$J(u) = D(u) + \alpha S[u]$$

where D is the similarity measurement function, S is the smoothing term that penalizes unlikely deformations, and u is the deformation field or other transform applied to the moving image [61]. The influence of the regularizer depends on the value of the scalar α.

Several optimization algorithms have been developed and validated for rigid and non-rigid ultrasound registration. We discuss the approaches proposed in the literature for rigid and non-rigid body transformations in the following subsections, which are summarized in Table 3.

Table 3
Optimizers used for ultrasound registration.

Registration type		Optimizer
Rigid Only	Adapted	Least-Squares optimization using Horn's Quaternion-based method [71], Nelder-Mead Simplex method [72], Mean-Shift optimization combined with Powell's direction set method [34]
Non-Rigid Only	Novel	Alpha-Expansion technique [73], Gradient Descent [63], Variational minimization [6,51]
	Adapted	Nelder-Mead Simplex method [20,34–36,38,62], Gradient Descent [37,64,73–75], Conjugate Gradient Descent [54], Least-Squares minimization [26], Levenberg- Marquardt optimization [75], Broyden-Fletcher-Goldfarb-Shannon (LBFGSB) optimizer [76]

4.1. Optimizers used only in rigid registration

In a rigid registration, similarity measurement can be considered as a 6 dimensional function due to the 6 degrees-of-freedom transformation. Since it is not possible to search through the entire parameter space exhaustively, initial parameter estimation is essential for the efficiency and accuracy of the optimization process.

4.1.1. Adapted

The most widely used optimization algorithm for rigid only ultrasound image registration is the simplex method of Nelder and Mead [19–22,55,72,77,78] due to its robustness and computational efficiency. Inspired by the concept of a simplex, the Nelder and Mead algorithm is commonly used to find the minimum or maximum of an objective function in a multidimensional space. Before determining the initial simplex, normalization is needed for both translations and rotations so that the unit step in parameter space is approximately the same as the displacement in the spatial domain. In order to avoid finding local minimums and maximums, the size of initial simplex should be greater than the unit dimension. To stop the optimization process, two conditions are considered. The first one is when the size of the simplex is smaller than a unit hypercube in the parameter space. The second one is when similarity measurement meets a pre-defined value [47].

In [34], a mean-shift based optimization algorithm was used with the Powell's direction set method [79]. There are two advantages to using the mean-shift algorithm: (1) the local fluctuation is eliminated on the surface of similarity function effectively, and (2) the optimization process can be robust and accurate using a multi-resolution approach. In a high dimensional space, the computational load will be reduced by using Powell's direction set method [34].

Another optimizer that has been validated with rigid body ultrasound registration is the least squares method [80]. Yip et al. [81] used Random Sample Consensus [82] (RANSAC) to reject outliers, and identify the best transformation for registration. The least squares optimization was performed using Horn's quaternion-based method [71].

4.2. Optimizers used only in non-rigid registration

4.2.1. Novel

In [25], the registration energy cost function was modeled using Markov Random Fields (MRF), and optimized using a parallelized alpha-expansion technique [73]. In [30], a fuzzy correspondence matrix was used in addition to the compatibility coefficient (see Section 3.3.1) in order to estimate the transformation that maps points in the moving ultrasound image to the fixed ultrasound image. The transformation was defined using the Thin Plate Spine (TPS) model. In [63], the optimizer of choice was a gradient descent optimizer with an automatic step-size update. This paper proposed a unique way of estimating the global spatio-temporal deformation field for a sequence of images using this optimization method and a B-spline parametric model. In [61], the cost function contained a diffusion regularizer, and a variational minimization approach was utilized in order to register the volumes together. Here, the cost function was minimized by applying calculus of variations to obtain a non-linear partial differential equation, which was then solved using the modified fix-point iteration with incremental updates being regularized [83]. A variational framework was also used in [6] to solve the problem of non-rigid ultrasound registration. Here, the cost function consisted of a data term and a smoothness term, which could be minimized for gradient descent using the Euler-Lagrange method. The Euler-Langrange equations that were derived in their paper were solved using an alternating minimization approach.

4.2.2. Adapted

In [48], first semi-automated approach was proposed (the authors did not know of any previously published semi- or fully automated algorithm) for non-rigid registration of ultrasound images of the breast. The optimizer used in this paper was the Nelder simplex algorithm [72]. The user clicked 3 control points in the moving image, and the optimizer tried to maximize the MI between the fixed and the moving images. The three control points were used to defined a standard rigid transform (rotate-translate), and the rigid transform defined an additional control point. The four control points were then used to estimate a full affine transform. Finally, the affine transform defined more points, which could in turn be used to estimate repeated TPS warps.

In [24], a sub-volume based volumetric registration (SURE) algorithm was proposed, which divided the three-dimensional volume into subvolumes. They then proceeded to compute the similarity of each subvolume to the target volume within a search window, while discarding non-matching subvolumes. Finally, they computed the translation only vector to target volume, and then used the TPS model to estimate the deformation field between original position of subvolumes and new position of subvolumes. The optimizer they used in this paper was the Nelder-Mead simplex method [72]. In [47], a modified version of the Nelder-Mead simplex method proposed in [21] was utilized.

In [50], the MIAMI-FUSE registration software [84] was utilized for non-rigid ultrasound volume registration of the breast. Initially, affine registration was done by manually selecting control points. After initial alignment, at least one additional control point was needed for elastic registration using TPS. The location of other grayscale voxels in the moving volume was interpolated using TPS, and the three-dimensional volumes were registered. Nelder-Mead simplex method [72] was used for optimization of the cost function.

In [54], a Bayesian regularization framework for non-linear registration was proposed with the minimization achieved through conjugate gradient descent. The deformation field was generated by fitting a cubic tensor product B-spline approximating mesh.

A non-rigid registration algorithm was proposed in [49] that operated by optimizing a cost function made up of global and local motion models. The global motion model described the motion of the brain using an affine transform. The local motion model was based on the B-spline free form deformation (FFD). They used a multi-resolution approach in order to estimate the FFD from coarse-to-fine levels. They used the gradient descent optimizer proposed in [74].

In [85], an approach was put forth which was an extension of the demons algorithm. They added an extra force to the optical flow equation of the demons algorithm called the inertia force. By adding this extra term, they were able to achieve better non-rigid registration results over the traditional demons algorithm. The optimizer used here was a second order gradient descent on the SSD criterion.

A near real-time algorithm (RESOUND) was put forth in [27] that incorporated the minimization a cost function comprised of a similarity term based on NCC, and a smoothness term. The deformation field was estimated using cubic B-splines. The optimization was done by taking the analytic derivative of NCC, and using a stochastic gradient descent algorithm as in [86,87]. The algorithm was implemented over a three level multi-resolution framework.

An algorithm was implemented in [67] that registered an entire 4D (3D + time) sequence of liver ultrasound volumes in a group-wise fashion, and avoided bias towards a specifically chosen reference time point. The algorithm utilized the 4D FFD B-spline model

in order to estimate the deformation field. The optimizer that was used in this paper was the stochastic gradient descent algorithm [86,87], and the parameters for this algorithm were from the elastix toolbox [88]. The algorithm was executed using a multi-resolution approach.

A multi-resolution approach was proposed in [4] that had an embedded multi-grid registration framework. This meant that they divided a volume into partitions at each level. At each of the various scales, the image was divided into specific sub blocks within the same grid, and the deformation field was estimated for that block in the grid. Then, for a cube at each grid level, a 12-parametric increment field was estimated. The deformation field at the grid level was then used to initialize the deformation field over the next grid level. The optimizer used here was a multi-grid reweighted least squares minimization algorithm employing an iterative Gauss-Seidel scheme [26].

In [5], an algorithm for Intra-Vascular Ultrasound (IVUS) image registration was implemented by transforming the images from image coordinates into polar coordinates. Here, the registration energy functional to be minimized comprised the sum of squared differences of intensities, and the sum of squared differences in radial gradient in each pixel of the region of interest (ROI). The minimization was done based on the Levenberg-Marquardt optimization [75]. Bicubic B-splines were used to represent the deformation field.

In [52], a non-rigid registration algorithm was proposed which incorporated a twisting and bending model. They used the Powell optimizer [77,79] to estimate the six parameters of the rigid transformation along with the six parameters of the non-rigid transform. This optimizer did not require the calculation of gradient parameters in order to perform the optimization, and hence it was a suitable choice in this paper.

In [17], two methods were utilized to extract point pair correspondences describing the shape of objects in ultrasound images. First, they employed a global shape extraction scheme through segmentation to generate point pair correspondences between the fixed and moving images. Then, they used SIFT feature detection and matching to obtain salient feature points that defined the structure of the object of interest in the image. They used the point pair correspondences generated from the two aforementioned steps in a Bayesian framework, where the displacement field was estimated using MAP framework. The fast optimization algorithm proposed in [89] to obtain the velocity field by simple scale-space convolution was used for registering the images together.

Similarly, the method proposed in [35] utilized SIFT-based feature detection and matching at a single scale to register volumes. The volumes were acquired with small displacements, which allowed them to adopt a Register-To-Global strategy where features detected in newly acquired volumes were registered to a combination of features from all previous volumes encountered in the sequence. Their group-wise registration scheme was faster than [36,37], while maintaining accuracy.

The algorithm in [62] used the diagonal (d), vertical (v), and horizontal (h) components of the discrete Meyer wavelet transform to generate energy maps. They applied wavelet decomposition through a multi-resolution approach, minimized an energy functional with SSD as similarity metric and diffusion regularizer. They used the calculus of variations to minimize the energy functional leading to the Euler-Lagrange equation. This equation was approximated as a linear system by a finite difference method. The fixed point iteration method was used to find the approximate solution of this linear system.

Inter-session registration of three-dimensional *trans*-rectal ultrasound (TRUS) was achieved in [51]. They utilized two different non-rigid algorithms for comparison of performance. The first was surface-based registration using an initial ICP-based rigid registration of three-dimensional TRUS volumes followed by non-rigid registration using TPS [90]. The second was image-based registration with a block matching approach [91] with MI as the similarity metric, followed by non-rigid registration using cubic B-splines. The optimizer that was used here was the Broyden-Fletcher-Goldfarb-Shannon (LBFGSB) optimizer [76].

A non-rigid registration algorithm was proposed in [60] to track the mitral valve annulus in three-dimensional ultrasound volumes. The optimizer that was used in this algorithm was the LBFGSB optimizer. The deformation field was estimated using three-dimensional third order B-splines. A multi-resolution approach was used.

An algorithm was proposed in [32] that registered volumes through the use of a model-based segmentation. They created a model of the aortic root by manually segmenting three-dimensional volumes of pediatric patients. Next, they acquired new 4D echo images of pediatric hearts, from which two three-dimensional volumes were extracted, and set as the reference and target respectively. These volumes were segmented using the deformable aortic root model that was generated. Next, 3D meshes were generated from the segmentations of the three-dimensional volumes. The three-dimensional meshes were then registered using TPS, thereby registering the extracted three-dimensional echo volumes.

A two-step approach was developed in [53] for elastic registration of IVUS frames in a sequence. First, rigid registration was performed to align coronary artery IVUS ultrasound B-scans. Then, the lumen contour was detected, and the IVUS image was transformed into polar coordinates. Finally, TPS interpolation was used for elastic registration of the lumen contour points detected between successive two frames in a sub-sequence.

An alternating minimization strategy that was proposed in [92] was utilized in [93] for the registration of pre- and post-biopsy volumes. The cost function that was proposed in [54,66] was modified, and utilized in [14–16,65,70], and there was no optimization performed in these implementations.

5. Registration techniques and results by anatomy

Ultrasound imaging has been used to image different organs of the human body over the past decades. In the following sections, the results of ultrasound-to-ultrasound (monomodal) registration algorithms are discussed based on the type of organ or anatomy for which they were implemented and validated. Table 4 summarizes some key anatomic results and references.

5.1. Head

In [34], a novel robust method is presented to register three-dimensional ultrasound fetal head images. They used Gabor filters

Table 4
Representative ultrasound registration systems for specific anatomy.

Anatomy	Reference	Registration type	Accuracy of results
Head	[34]	3D Rigid	92% successful registration
Neck	[64]	2D Rigid	5.1 pixel registration error
Breast	[50]	3D Non-Rigid	1.2 ± 0.9 mm
Heart	[53]	2D Non-Rigid	0.5 ± 1.535 pixels
Liver	[62]	2D Non-Rigid	6.9700 pixels SSD error
Kidney	[30]	2D Non-Rigid	0.131 pixel RMS error
Gall bladder	[13]	3D Rigid	<10 mm registration error
Bone	[22]	3D/4D Rigid	<1 mm registration error
Prostate	[51]	3D Non-Rigid	1.96 ± 0.85 mm registration error
Fetal imaging	[25]	3D Non-Rigid	0.78 ± 0.633 mm mosaicking error

to extract textures and edge features, the correlation ratio as the similarity metric and a mean-shift based optimizer with Powell's direction set method. As a result, the proposed method was able to achieve a successful registration rate of 92% for large initial misalignment with correlation ratio metric. The algorithm was evaluated on two three-dimensional volumes of fetal heads. Among the different metrics that were used, CR performed the best with the greatest capture range.

The minimization of a non-rigid three-dimensional registration problem in a multi-resolution framework was done in [4]. The optimizer used in this approach was a multi-grid reweighted least squares minimization algorithm employing an iterative Gauss-Seidel scheme. They had applied their embedded multi-grid and multi-resolution approach on artificially deformed volumes of the brain of an 8-month old baby, and on the brain of a pig. With their regularized Perona and Malik (P&M) approach, they achieved a better metric score, lowering the baby-brain Mean Squared Error (MSE) metric score by about 5.7% and reducing the angular error by about 2.3% to 13.8°, in comparison to an approach that does not incorporate any multi-scale framework.

A non-rigid registration algorithm designed in [49] that was applied to three-dimensional ultrasound volumes acquired before and after opening the dura of the brain of two patients with brain tumors. The algorithm operated by optimizing a cost function made up of global and local motion models. They used the gradient descent optimizer proposed in [74] to minimize the cost function. The results before and after registration were compared; the registration method involved an affine plus free-form deformation (FFD) with a control point spacing of 4. They computed the overlap of the segmented tumor volume before and after registration, and found that the overlap after registration jumped to 96% from a 76% overlap before registration. Fig. 1 shows results that the affine registration is applied to ultrasound volume after opening the dura.

A near real-time registration algorithm (RESOUND) was developed in [27] for registering ultrasound volumes acquired before and after the resection of brain tumors. The algorithm incorporated the minimization a cost function comprised of a similarity term based on NCC, and a smoothness term. The optimization was done by taking the analytic derivative of NCC, and using a stochastic gradient descent algorithm as in [86,87]. The deformation field was estimated using cubic B-splines. The authors validated their results by manually providing corresponding landmarks in each volume, and compared the volumes before and after registration by estimate the mean target registration error. The initial error before registration was 3.7 mm, while the error after registration dropped to 1.58 mm.

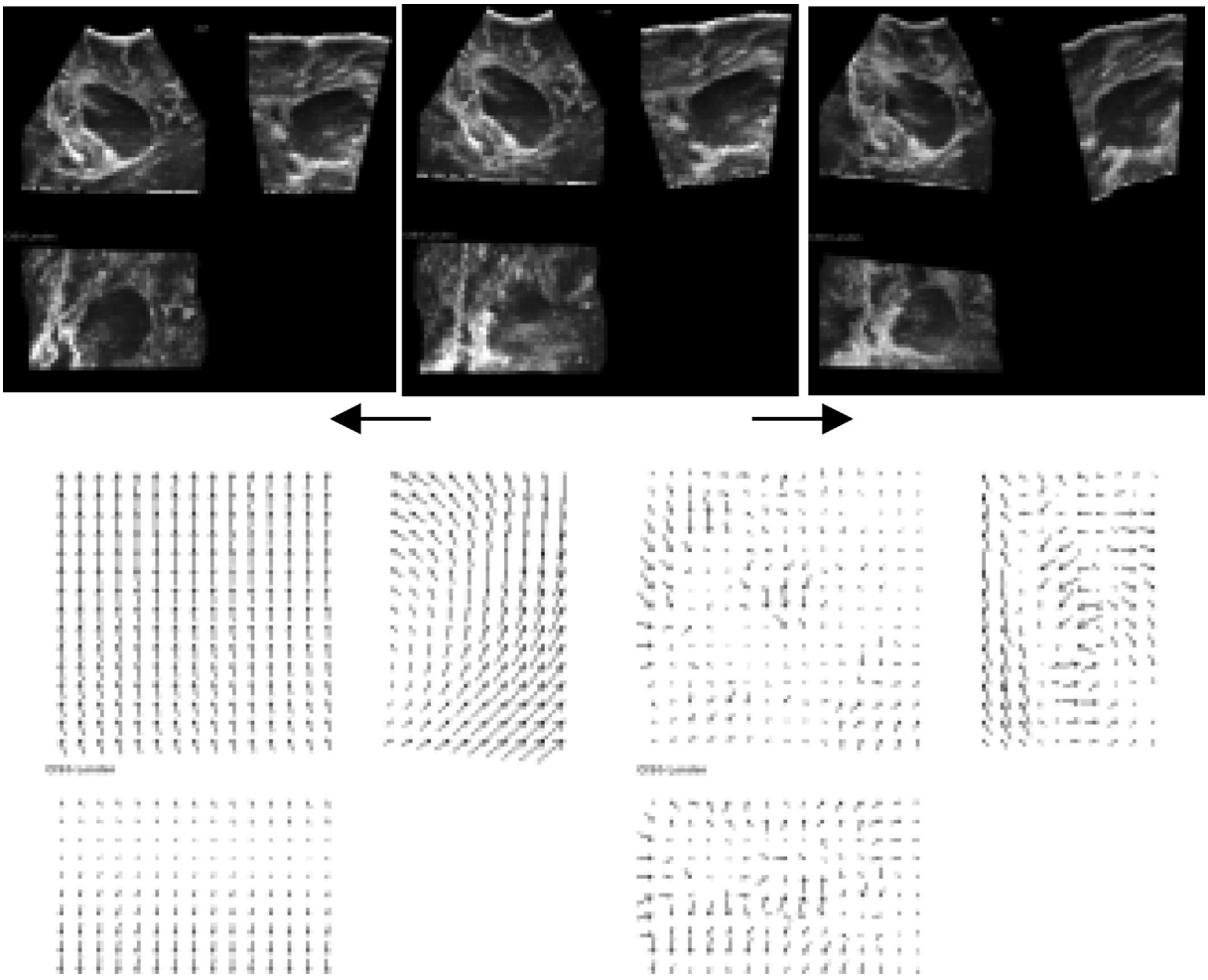

Fig. 1. Deformation field. **Top:** left: Ultrasound volume after opening the dura, middle: Ultrasound volume after opening the dura + affine registration, right: Ultrasound volume before opening the dura. **Bottom:** left: Deformation field for affine registration, right: Deformation field for free-form deformation (control point spacing 4 mm) without the affine component. (Medical Image Computing and Computer-Assisted Intervention – MICCAI 2003, Non-rigid Registration of 3D Ultrasound Images of Brain Tumours Acquired during Neurosurgery, Volume 2879, 2003, p414, Marloes M. J. Letteboer, Peter W. A. Willems, Max A. Viergever, and Wiro J. Niessen, © Springer-Verlag Berlin Heidelberg 2003, with permission of Springer.) [49].

5.2. Neck

In [64], a novel hybrid procedure for registering envelop detected radio frequency ultrasound data of human neck was proposed, using global statistics and local textural features. Globally, Hellinger distance between distributions is utilized and Fuzzy Local Binary Patterns (FLBP) is used on a local scale to perform registration. As a result, the median registration error on five datasets using the methodology put forth in [64] is much lower than other similarity measures such as SSD and NCC.

5.3. Breast

In [54], a fully automated non-rigid registration algorithm was proposed for registering free-hand ultrasound volumes of the female breast. A Bayesian regularization framework incorporating a block matching scheme was developed with the minimization achieved through conjugate gradient descent. The deformation field was generated by fitting cubic tensor product B-spline meshes. The boundary of the cysts and background texture were well preserved in in vivo ultrasound images of the breast after registration. Fig. 2 shows results of registering and compounding two sweeps of a breast fibroadenoma.

A sub-volume based volumetric registration (SURE) algorithm was developed in [24], which was used to register synthetically warped ultrasound volumes of the female breast. The algorithm used the TPS model to estimate the deformation field between original position of subvolumes and new position of subvolumes. The optimizer they used in this paper was the Nelder-Mead simplex method [72]. The synthetic deformations that were applied to a reference volume were in the range of 1.5–2.5 mm, and this was reduced by over 85% when using their registration algorithm. This was significantly higher than the 59% and 50% reduction in deformation obtained by using rigid and affine transforms respectively.

In [48], the first semi-automated approach was proposed for non-rigid registration of ultrasound images of the breast. The optimizer used in this paper was the Nelder simplex algorithm. TPS warps were computed by having the user manually click control points in the moving image, and using the optimizer to maximize the MI between the fixed and the moving images. They prove that their algorithm achieves a 27% increase in mutual information by using the nine point TPS solution over the full affine registration.

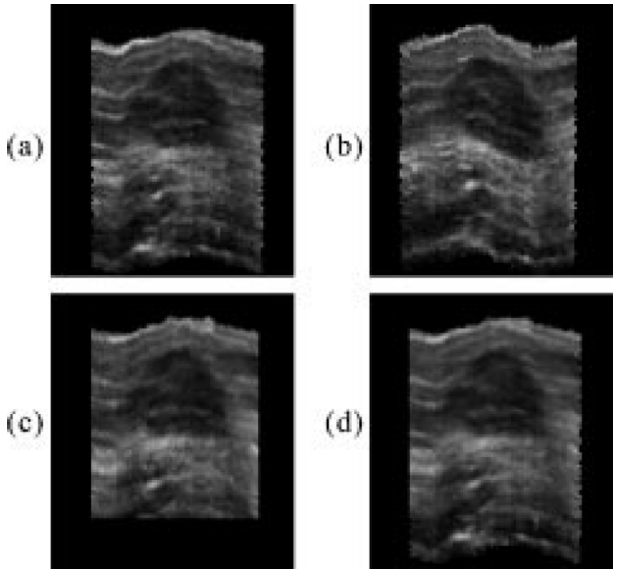

Fig. 2. Registration and compounding of two sweeps of a breast fibroadenoma. (a) Sweep 1 (the reference image). (b) Sweep 2 (the floating image). (c) The result of registering Sweep 2 to Sweep 1. (d) Compounding of Sweep 1 and 2 after registration. © [2002] IEEE. Reprinted, with permission, from [54].

In [50], the MIAMI-FUSE registration software [84] was utilized for non-rigid ultrasound volume registration of the female breast. Initially, affine registration was done by manually selecting control points. After initial alignment, at least one additional control point was needed for elastic registration using TPS. The location of other grayscale voxels in the moving volume was interpolated using TPS, and the three-dimensional volumes were registered. Nelder-Mead simplex method was used for optimization of the cost function. The algorithm successfully registered automated whole breast ultrasound (ABU) volumes, and reduced the mean registration between manually annotated landmark points after registration to 1.2 ± 0.9 mm.

In [85], an approach was put forth which was an extension of the demons algorithm. They added an extra force to the optical flow equation of the demons algorithm called the inertia force. By adding this extra term, they were able to achieve better non-rigid registration results over the traditional demons algorithm. The optimizer used here was a second order gradient descent on the SSD criterion. The paper showed that the SSD ratio computed over multiple iterations dropped quickly and was lower than comparable registration algorithms, thus indicating successful registration.

5.4. Heart

In [78], a registration framework was proposed to register real-time volume ultrasound images of the heart. This rigid registration framework is based on mutual information and uses Nelder-Mead method as an optimizer. Over a range of image sets and parameters, the reported translation error range was 0.32 mm to 2.58 mm, and the rotation error range was 0.17 degree to 9.25 degree.

In [19], a technique was developed to temporally align two sequences of pre-stress and post-stress three-dimensional images for stress echocardiography, followed by a spatial registration process. This registration uses mutual information as similarity metric and a downhill simplex method as optimizer. As a result, working with three-dimensional stress echocardiography it is shown that this registration framework can potentially "improve the diagnostic accuracy of stress testing".

In [5], an algorithm for Intra-Vascular Ultrasound (IVUS) image registration was implemented by transforming the images from image coordinates into polar coordinates. Here, the registration energy functional to be minimized comprised the sum of squared differences of intensities, and the sum of squared differences in radial gradient in each pixel of the region of interest (ROI). The minimization was done based on the Levenberg-Marquardt optimization [75]. The mean and standard deviation for the X error with a control point spacing sequence (CPSS) of 30–20, and a weighting coefficient of 0.5 was 0.023 ± 0.156 pixels.

In [63], the paper proposed a unique way of estimating the global spatio-temporal deformation field for a sequence of left ventricle ultrasound images using a gradient descent optimization method and a B-spline parametric model. In the ultrasound sequence containing realistic noise, the geometric error in pixels was 1.265 pixels (corresponding to 5% displacement). This result suggests that the spatio-temporal algorithm works better than a previously published algorithm in [94].

In [52], a non-rigid registration algorithm was proposed which incorporated a twisting and bending model to register three-dimensional volumes of the carotid artery. They used the Powell optimizer [58,60] to estimate the six parameters of the rigid

transformation along with the six parameters of the non-rigid transform. The overall mean and standard deviation for the mean registration error between the fixed and moving volumes was 1.03 ± 0.23 mm for non-rigid registration over 1.50 ± 0.50 mm for rigid registration.

A variational framework was used in [6] to solve the problem of non-rigid ultrasound registration. Here, the cost function consisted of a data term and a smoothness term, which could be minimized for gradient descent using the Euler-Lagrange method. The Euler-Langrange equations that were derived in their paper were solved using an alternating minimization approach. The SSD between the fixed and moving images after intensity-based registration algorithm was 37.37 pixels, while the SSD after intensity + local phase information based non-rigid registration was 34.76 pixels.

An algorithm that registered three-dimensional volumes through the use of an aortic root model-based segmentation was described in [32]. The performance of the registration algorithm was illustrated by the use of the Canny edge detector to extract boundaries in the image sets, and it was clear that the algorithm did well in aligning the edges and boundaries in the images.

A multi-resolution non-rigid registration algorithm was developed in [60] to track the mitral valve annulus in three-dimensional ultrasound volumes. The optimizer that was used in this algorithm was the LBFGSB optimizer. The deformation field was estimated using three-dimensional third order B-splines. The tracking algorithm produced an average root mean squared error (RMSE) of 1.96 ± 0.46 mm over all the datasets. The same non-rigid registration algorithm was also used in [33,56–59].

A two-step algorithm for elastic registration of IVUS frames in a sequence was developed in [53]. First, rigid registration was performed to align coronary artery IVUS ultrasound B-scans. Then, the lumen contour was detected, and the IVUS image was transformed into polar coordinates. Finally, TPS interpolation was used for elastic registration of the lumen contour points detected between successive two frames in a sub-sequence. The elastic registration error was measured between five image pairs and compared against the iterative closest point (ICP) algorithm [95]. The mean and standard deviation of the elastic registration error of one image pair was 0.519 ± 1.464 pixels, and this was lower than the ICP-based registration error 0.778 ± 2.327pixels.

5.5. Liver

In [55], a methodology for image-based real time tracking for 4D ultrasound data was proposed using rigid image registration to deduce the positioning of each ultrasound frame in a global coordinate system. They used sum of squared differences (SSD) as similarity metric, a non-linear Nelder-Mead algorithm as optimizer and validated their methodology using liver scan. As a result, they proved that their method is able to provide results in agreement with previously developed magnetic-based tracking technique, which is widely used in clinical industry nowadays.

In [20], a registration framework was developed using mutual information to register 2-D liver images rigidly. Dividing rectangles and Nelder-Mead method are used as optimization algorithm. The results demonstrate that their automatic registration framework can reach minimum value of 0.719 and 0.98 using DIRECT and Nelder-Mead methods respectively after 50 iterations. Thus it is accurate, robust and well suited for clinical applications.

In [96], a fast affine registration framework was developed to compensate in real-time for liver three-dimensional motion/displacement due to breathing using block-matching method. Normalized cross correlation is used as similarity metric. The optimization problem is mapped from non-homogeneous to homogeneous and solved by using replicator dynamics efficiently. Validation was performed on 91 subjects, with two ultrasound volumes from each, with a "mean registration error of 1.8 mm".

The diagonal (d), vertical (v), and horizontal (h) components of the discrete Meyer wavelet transform was used in [62] to generate energy maps from liver ultrasound images. They minimized the energy functional with SSD as similarity metric and diffusion regularizer. They used fixed point iteration method as the optimizer. The algorithm outperformed an intensity-based registration with a SSD of 6.97 over 29.7 for the intensity-based registration.

An algorithm was implemented in [67] that registered an entire 4D (three-dimensional + time) sequence of liver ultrasound volumes in a group-wise fashion, and avoided bias towards a specifically chosen reference time point. The optimizer that was used in this paper was the stochastic gradient descent algorithm, and the parameters for this algorithm were from elastix toolbox [88]. Their paper showed that the average 75% percentile of the registration error (1.0 mm) is lower than the average 75% percentile of the bias-corrected inter-observer error (1.4 mm).

In [61], the non-rigid registration algorithm utilized a cost function that had a diffusion regularizer, and a variational minimization approach was used to register the three-dimensional volumes of the liver together. Here, the cost function was minimized by applying calculus of variations to obtain a non-linear partial differential equation, which was then solved using the modified fix-point iteration with incremental updates being regularized [83]. The gain in similarity was measured by computing the ratio of the differences in similarity before and after registration to the original similarity. For the SSD, the ratio ranged between 32.82% and 48.47% with an average of 40.78% for 5 datasets.

A three-dimensional registration algorithm was implemented in [15] to register human liver volumes using a novel similarity metric defined in Section 3.3.1 and a cost function that was proposed in [54,66]. For validation of the results, they manually selected points in the fixed and moving data sets, and estimated the distance between them after automatic registration. The error was about 1.4 mm. Similar results were proposed in [14,16,65,70].

5.6. Kidney

In [17], point pair correspondences were extracted that described the shape of objects in ultrasound images, and then used in a Bayesian framework, where the displacement field was estimated using MAP framework. The fast optimization algorithm proposed in [89] to obtain the velocity field by simple scale-space convolution was used for registering the images together. They achieved a cross-correlation (CC) value of 0.979 by using their registration algorithm over the CC value of 0.92 before registration. See in Fig. 3.

In [30], a fuzzy correspondence matrix was used in addition to the compatibility coefficient (see Section 3.3.1) in order to estimate the transformation that maps points in the moving ultrasound image to the fixed ultrasound image. The transformation was defined using the Thin Plate Spine (TPS) model. The mean Root Mean Square (RMS) error in a 9 frame separation was 1.31×10^{-1}, compared to 2.22×10^{-1} in TPS – Robust Point Matching (TPS – RPM) proposed in [97].

5.7. Gall bladder

In order to accurately perform three-dimensional spatial compounding for improvement in quality of ultrasound data, [13] adapted a previously developed multi-model CT to MRI registration algorithm to three-dimensional ultrasound data. Using a multi-resolution approach, they developed a correlation-based registration framework and it has been validated with gall bladder

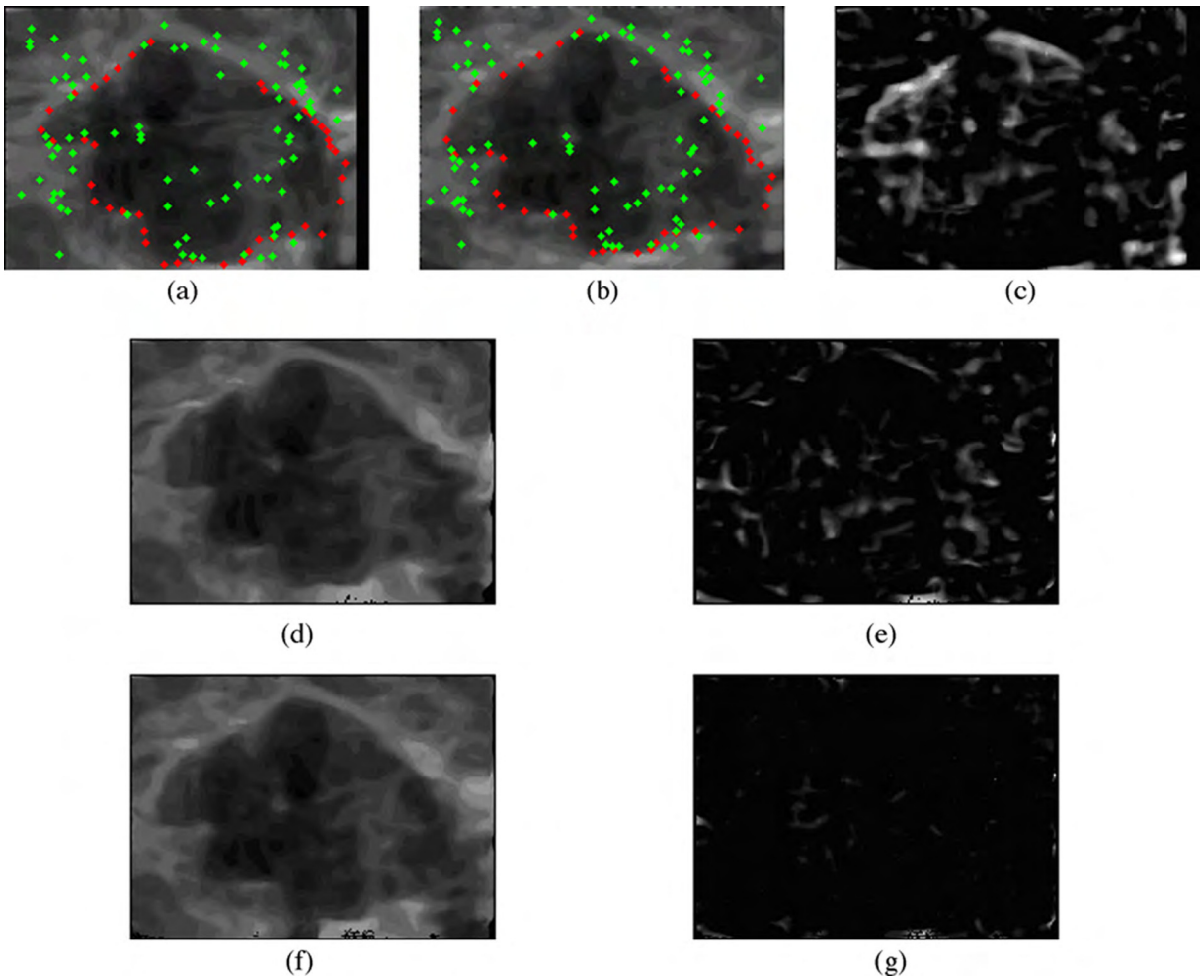

Fig. 3. (a) The template image (220 × 160) with 135 landmark points. (b) The target image (220 × 160) with 135 landmark points. (c) The difference image between template and target images. (d) The deformed template image using Christensen's fluid method. (e) The difference image between d and b. (f) The deformed template image using [the] method. (g) The difference image between (f) and (b). Reprinted from Publication [17] with permission from Elsevier.

ultrasound data. As a result, the rigid registration translational and rotational errors are approximately maintained within 10 mm and 10 degrees for a total of 600 B-scans.

5.8. Bone

In [22], a method was developed for 3D/4D ultrasound registration of the bone in order to reduce the invasiveness of Computer Assisted Orthopaedic Surgery (CAOS). Normalized cross correlation is used as similarity metric and the simplex method of Nelder and Mead is selected for optimization process. As results, 65% of the cases show a successful registration result with average time of 10 s for each.

5.9. Prostate

Inter-session registration of three-dimensional *trans*-rectal ultrasound (TRUS) was achieved in [51]. They utilized two different non-rigid algorithms for comparison of performance. The first was surface-based registration using an initial ICP-based rigid registration of three-dimensional TRUS volumes followed by non-rigid registration using TPS. The second was image-based registration with a block matching approach with MI as the similarity metric, followed by non-rigid registration using cubic B-splines. The optimizer that was used here was the Broyden-Fletcher-Goldfarb-Shanon (LBFGSB) optimizer [76]. The pre-registration mean target registration error (mTRE) for the whole gland was 7.36 ± 4.17 mm, while the mTRE after non-rigid image-based registration was 1.96 ± 0.85 mm. Results are shown in Fig. 4.

For the guidance of needle biopsies in prostate image-guided radiation therapy, an alternating minimization strategy that was proposed in [92] was utilized in [93]. The algorithm used B-splines in order to transform and register the post-biopsy volumes to the pre-biopsy volumes. In [46], three registration methods were evaluated for the registration of three-dimensional-transabdominal ultrasound volumes. These volumes were acquired for the setup of postprostatectomy patients during radiation therapy. The similarity metric used for the registration was mutual information, and since they were only estimating translations, the three translation parameters were optimized using the adaptive stochastic gradient descent optimizer [83].

5.10. Fetal imaging

In [25], the registration energy cost function was modeled using Markov Random Fields (MRF), and optimized using a parallelized alpha-expansion technique [73]. The clinical application of this paper was in the construction of fetal mosaics for use in a training simulator, the proposed method outperformed the spatial compounding techniques [98] that required almost perfect alignment between volumes. See Fig. 5.

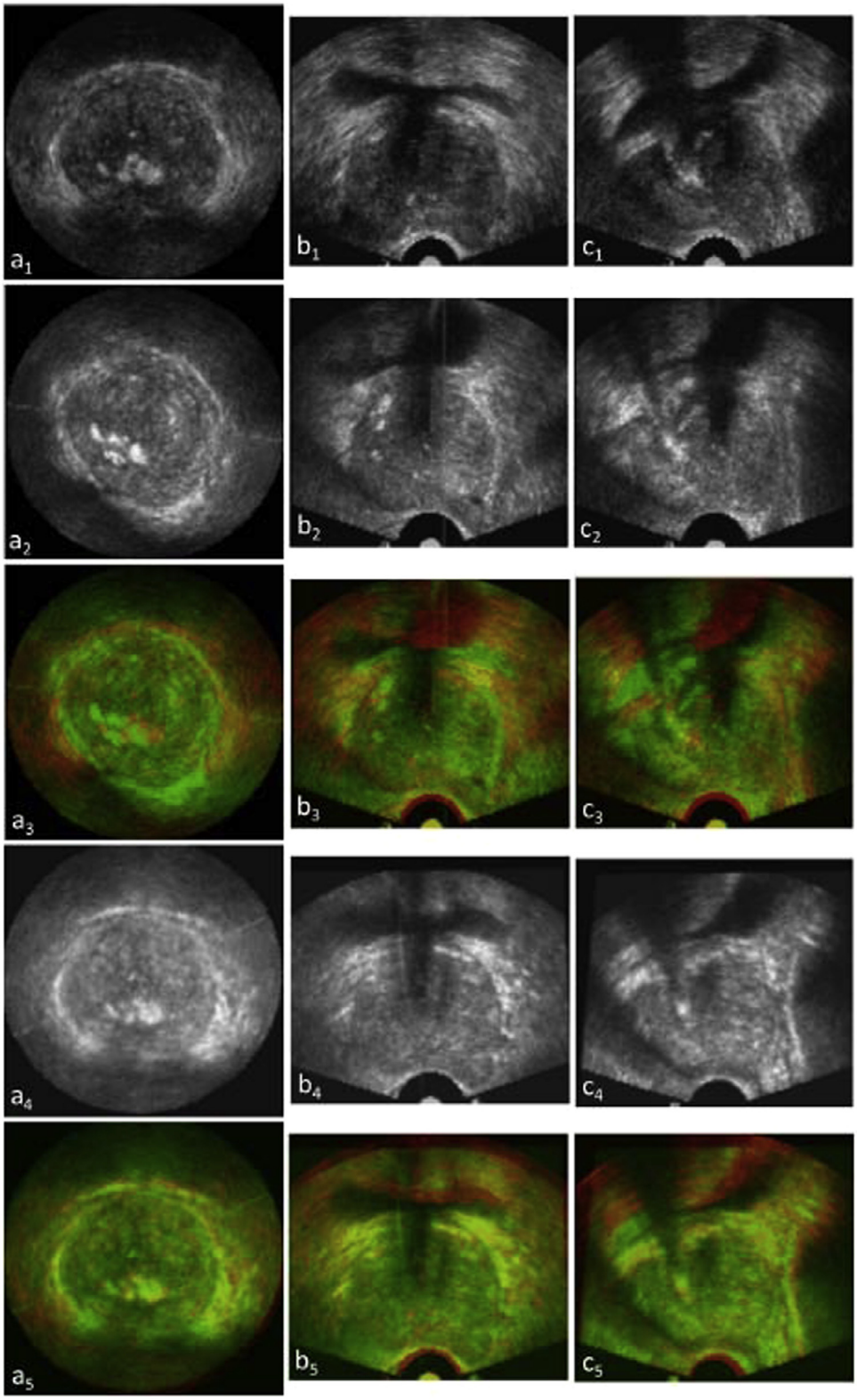

Fig. 4. Visual assessment of three-dimensional TRUS registration. a_1, b_1 and c_1 are post-biopsy images in three directions. a_2, b_2 and c_2 are pre-biopsy images, and a_3, b_3 and c_3 are the fusion images between pre- and post-biopsy images. a_4, b_4 and c_4 are the 3D registered pre-biopsy images; and a_5, b_5 and c_5 are the fusion images between registered pre- and post-biopsy images. Reprinted from Publication [93] with permission from SPIE.

6. Discussion, Shortcomings, and future opportunities

Many of the cited algorithms are freely available from the author's websites. An increasingly large number of registration algorithms also have free open-source implementations in the Insight Toolkit (ITK) [99] and its associated Insight Journal. Although a variety of mono-modality ultrasound registration frameworks were proposed and developed over the past few

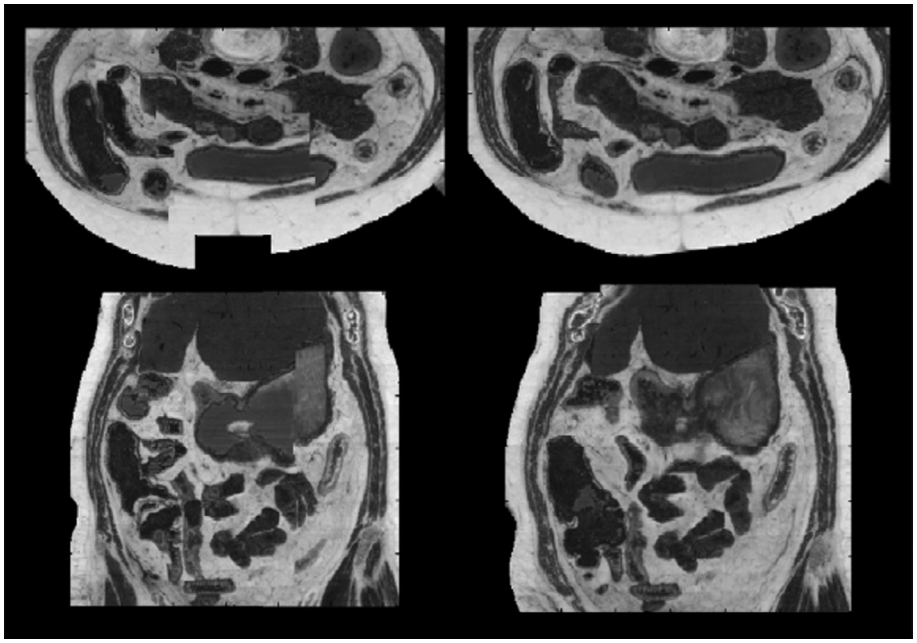

Fig. 5. Mosaicking of multiple volumes through the registration approach in [25]. The left half shows slices from the mosaiced volume when no registration is performed. The right half demonstrates how [the] algorithm can reconstruct the anatomy seamlessly, using multiple partially overlapping volumes. Reprinted from Publication [25] with permission from Elsevier.

decades, there are still shortcomings and unsolved issues in the field of ultrasound registration.

We have not summarized how rapidly, nor in what fraction of cases, reasonable non-rigid registration can be achieved. That assessment should be done periodically, particularly with continually evolving software packages such as commercial software.

Opportunities for future research are suggested below.

6.1. Diverse anatomy and ultrasound systems

With all the papers that have been reviewed, most registration frameworks were validated on human liver, cardiac and kidney anatomical structures. Ultrasound registration on other structures such as bone, bladder and peripheral anatomy are not as well studied, nor are animal models such as mice and pigs. More attention is needed on less common ultrasound configurations, such as intravascular acquisition or high-frequency small-animal imaging.

6.2. Interactive nature of ultrasound acquisition

As discussed in previous sections, ultrasound registration algorithms are robust to some changes, such as gain, focal depth etc. However, other differences remain problematic. Ultrasound is a uniquely interactive imaging modality. The probe is freely positioned during image acquisition, allowing imaging from different viewpoints while providing visual feedback that can be used to physically manipulate the patient (or animal). Careful manipulation and choice of viewpoint are often crucial to acquiring diagnostic quality images, leading to engineering complexities and untapped potential.

6.2.1. Physical probe tracking

In many clinical applications, free-hand ultrasound volumes are acquired, and the position of the ultrasound probe is tracked directly using either a magnetic or optical tracking system. However, existing probe tracking systems are somewhat restrictive and/or not extremely accurate. More importantly, the true three-dimensional location of the probe is obtained relative to the tracker's coordinate system, and not relative to the patient's anatomy. This can be a hindrance to the registration of images since the internal structures of the patient's anatomy can deform while being imaged, but the tracker cannot accurately quantify these movements as it provides only global motion estimates relative to the tracker coordinate system. Prior work has been done to instead directly track an ultrasound transducer relative to a patient's anatomy [8,35,100–103]. Most researchers use probe tracking as (an often poor) surrogate for rigid registration between consecutive images, in many cases followed by non-rigid registration as a fix-it step. However, given the under-constrained nature of non-rigid registration, it is preferable to begin with as accurate of a rigid transform as possible.

6.2.2. Viewpoint specific

Ultrasound allows image acquisition from different viewpoints. Even when imaging the same anatomy without any physical manipulation, different viewpoints will still produce different pixel intensities for the exact same micro-volume of tissue. Other effects such as refraction, visual occlusion and shadowing due to the complex internal tissue structures can make it difficult to register ultrasound images acquired from different viewpoints using only image-based approaches.

6.2.3. Interactive manipulation during ultrasound acquisition

Ultrasound imaging routinely requires physical manipulation of the subject being scanned, typically to visually judge the effects of compression or to push intervening anatomy out of the way. Often, the transducer itself is used as the primary manipulation device to compress or displace the tissue. Eventually, independent tracking of the ultrasound probe (as discussed in Section 6.2.1) might be used to generate good a priori models of deformation for use during non-rigid registration algorithms. To accurately predict both tissue compression and lateral tissue displacement, these models should take into account both the transducer's compression force and the total trajectory the transducer has followed. Open problems include continuous measurement of transducer compression, tracking the trajectory of the transducer relative to the anatomy,

and building predictive models from these measurements. With 2D array transducers, which are capable of real-time 3D acquisition, live tracking of tissues in the images between acquired image volumes may also provide useful preregistration.

Acknowledgements

This review was funded in part by U.S. National Institutes of Health R01 grant 1R01EY021641, U.S. National Library of Medicine contract HHSN27620100058OP, and U.S. Department of Defense Peer Reviewed Medical Research Program award PR130773 (HRPO Log No. A-18237).

References

[1] T. Selbekk, A.S. Jakola, O. Solheim, T.F. Johansen, F. Lindseth, I. Reinertsen, G. Unsgård, Ultrasound imaging in neurosurgery: approaches to minimize surgically induced image artefacts for improved resection control, Acta Neurochir. (Wien) 155 (2013) 973–980, http://dx.doi.org/10.1007/s00701-013-1647-7.

[2] U. Wagnetz, M. Atri, C. Massey, A.C. Wei, U. Metser, Intraoperative ultrasound of the liver in primary and secondary hepatic malignancies: comparison with preoperative 1.5-T MRI and 64-MDCT, Am. J. Roentgenol. 196 (2011) 562–568, http://dx.doi.org/10.2214/AJR.10.4729.

[3] K.L. Hansen, M.M. Pedersen, H. Møller-Sørensen, J. Kjaergaard, J.C. Nilsson, J.T. Lund, J.A. Jensen, M.B. Nielsen, Intraoperative cardiac ultrasound examination using vector flow imaging, Ultrason. Imaging 35 (2013) 318–332, http://dx.doi.org/10.1177/0161734613505552.

[4] I. Pratikakis, C. Barillot, P. Hellier, E. Memin, Robust multiscale deformable registration of 3d ultrasound images, Int. J. Image Graphics 3 (2003) 547–565.

[5] K. Oakeson, Quantification of cross-sectional artery wall motion with IVUS image registration, Med. Imaging 2004 (5373) (2004) 119–130, http://dx.doi.org/10.1117/12.536523.

[6] J. Woo, B.W. Hong, C.H. Hu, K.K. Shung, C.C.J. Kuo, P.J. Slomka, Non-rigid ultrasound image registration based on intensity and local phase information, J. Signal Process. Syst. 54 (2009) 33–43, http://dx.doi.org/10.1007/s11265-008-0218-2.

[7] R.C.G. Martin, D.A. North, Enhanced ultrasound with navigation leads to improved liver lesion identification and needle placement, J. Surg. Res. 200 (2015) 420–426, http://dx.doi.org/10.1016/j.jss.2015.09.003.

[8] J. Wang, V. Shivaprabhu, J. Galeotti, S. Horvath, V. Gorantla, G. Stetten, Towards Video Guidance for Ultrasound, Using a Prior High-Resolution 3D Surface Map of the External Anatomy, 2014, pp. 51–59.

[9] J. Ashburner, K. Friston, Rigid Body Registration and Interpolation, in: Hum. Brain Funct., Second ed., 2003, pp. 635–653, http://dx.doi.org/10.1016/B978-012264841-0/50034-2.

[10] M. Sarode, P. Deshmukh, Reduction of speckle noise and image enhancement of images using filtering technique, Int. J. Adv. Technol. 2 (2011) 30–38. http://www.ijict.org/index.php/ijoat/article/viewArticle/speckle-noise.

[11] K.W.J, Segen, M. Kulbacki, Optimization of joint detector for ultrasound images using mixtures of image feature descriptors, in: Lect. Notes Comput. Sci. (Including Subser. Lect. Notes Artif. Intell. Lect. Notes Bioinformatics), vol. 9012, 2015, pp. 1–2. http://dx.doi.org/10.1007/978-3-319-15705-4.

[12] A.H. Gee, G.M. Treece, R.W. Prager, C.J.C. Cash, L. Berman, Rapid registration for wide field of view freehand three-dimensional ultrasound, IEEE Trans. Med. Imaging 22 (2003) 1344–1357, http://dx.doi.org/10.1109/TMI.2003.819279.

[13] R.N. Rohling, A.H. Gee, L. Berman, Automatic registration of 3-D ultrasound images, Ultrasound Med. Biol. 24 (1998) 841–854. http://www.sciencedirect.com/science/article/pii/S030156299700210X.

[14] S. Khallaghi, C.G.M. Leung, K. Hastrudi-Zaad, P. Foroughi, C. Nguan, P. Abolmaesumi, Experimental validation of an intrasubject elastic registration algorithm for dynamic-3D ultrasound images, Med. Phys. 39 (2012) 5488–5497, http://dx.doi.org/10.1118/1.4742056.

[15] P. Foroughi, P. Abolmaesumi, K. Hashtrudi-Zaad, Intra-subject elastic registration of 3D ultrasound images, Med. Image Anal. 10 (2006) 713–725, http://dx.doi.org/10.1016/j.media.2006.06.008.

[16] C. Leung, K. Hashtrudi-Zaad, P. Foroughi, P. Abolmaesumi, A real-time intrasubject elastic registration algorithm for dynamic 2-D ultrasound images, Ultrasound Med. Biol. 35 (2009) 1159–1176, http://dx.doi.org/10.1016/j.ultrasmedbio.2008.12.018.

[17] X. Lu, S. Zhang, W. Yang, Y. Chen, SIFT and shape information incorporated into fluid model for non-rigid registration of ultrasound images, Comput. Methods Programs Biomed. 100 (2010) 123–131, http://dx.doi.org/10.1016/j.cmpb.2010.03.005.

[18] B. Wang, Y. Shen, A method on calculating high-dimensional mutual information and its application to registration of multiple ultrasound images, Ultrasonics 44 (2006).

[19] R. Shekhar, V. Zagrodsky, M.J. Garcia, J.D. Thomas, Registration of real-time 3-D ultrasound images of the heart for novel 3-D stress echocardiography, IEEE Trans. Med. Imaging 23 (2004) 1141–1149, http://dx.doi.org/10.1109/TMI.2004.830527.

[20] S.R.R. Suganya, R. Kirubakaran, Registration of ultrasound liver images using mutual information technique, Adv. Intell. Syst. Comput. 246 (2014) 155–162, http://dx.doi.org/10.1007/978-81-322-1680-3.

[21] V. Zagrodsky, R. Shekhar, J.F. Cornhill, Multi-Function Extension of Simplex Optimization Method for Mutual Information-Based Registration of Ultrasound Volumes, Image (Rochester, N.Y.), vol. 4322, 2001, pp. 508–515. http://dx.doi.org/10.1117/12.431124.

[22] J. Schers, J. Troccaz, V. Daanen, C. Fouard, C. Plaskos, P. Kilian, 3D/4D ultrasound registration of bone, Proc. – IEEE Ultrason. Symp., 2007, pp. 2519–2522. http://dx.doi.org/10.1109/ULTSYM.2007.634.

[23] P. Perona, J. Malik, Scale-space and edge detection using anisotropic diffusion, IEEE Trans. Pattern Anal. Mach. Intell. 12 (1990) 629–639, http://dx.doi.org/10.1109/34.56205.

[24] J.F. Kruecker, G.L. LeCarpentier, J.B. Fowlkes, P.L. Carson, Rapid elastic image registration for 3-D ultrasound, IEEE Trans. Med. Imaging 21 (2002) 1384–1394.

[25] J. Kutarnia, P. Pedersen, A Markov random field approach to group-wise registration/mosaicing with application to ultrasound, Med. Image Anal. 24 (2015) 106–124, http://dx.doi.org/10.1016/j.media.2015.05.011.

[26] E. Memin, P. Perez, Dense estimation and object-based segmentation of the optical flow with robust techniques, IEEE Trans. Image Process. 7 (1998) 703–719, http://dx.doi.org/10.1109/83.668027.

[27] H. Rivaz, D.L. Collins, Near real-time robust non-rigid registration of volumetric ultrasound images for neurosurgery, Ultrasound Med. Biol. 41 (2015) 574–587, http://dx.doi.org/10.1016/j.ultrasmedbio.2014.08.013.

[28] N. Otsu, A threshold selection method from gray-level histograms, IEEE Trans. Syst. Man. Cybern. 9 (1979) 62–66, http://dx.doi.org/10.1109/TSMC.1979.4310076.

[29] J. Canny, A computational approach to edge detection, IEEE Trans. Pattern Anal. Mach. Intell. 8 (1986) 679–698, http://dx.doi.org/10.1109/TPAMI.1986.4767851.

[30] J.-H. Lee, Y.K. Seong, M. Park, K.-G. Woo, J. Ku, H.-J. Park, Non-rigid ultrasound image registration using generalized relaxation labeling process, Image Process. Mach. Vis. Appl. VI 8661 (2013) 1–6, http://dx.doi.org/10.1117/12.2003233.

[31] S. Menet, P. Saint-Marc, G. Medioni, B-Snakes: Implementation and Application to Stereo, 1990.

[32] B. Matinfar, L. Zagorchev, Non-rigid Registration of 3D Ultrasound Images Using Model-based Segmentation, in: Proc. IEEE Conf. on Computer Vision and Pattern Recognition Workshops, 2014, pp. 323–328. http://dx.doi.org/10.1109/CVPRW.2014.132.

[33] B. Heyde, M. Alessandrini, J. Hermans, D. Barbosa, P. Claus, D. Jan, Conservation to Assess Cardiac Deformation From 3D Ultrasound Recordings, vol. 35, 2016, pp. 501–511.

[34] F. Cen, Y. Jiang, Z. Zhang, H.T. Tsui, T.K. Lau, Robust Registration of 3-D Ultrasound Images Based on Gabor Filter and Mean-Shift Method, 2004, pp. 304–316.

[35] R.J. Schneider, D.P. Perrin, N.V. Vasilyev, G.R. Marx, P.J. Del Nido, R.D. Howe, Real-time image-based rigid registration of three-dimensional ultrasound, Med. Image Anal. 16 (2012) 402–414, http://dx.doi.org/10.1016/j.media.2011.10.004.

[36] D. Ni, Y.P. Chui, Y. Qu, X. Yang, J. Qin, T.T. Wong, S.S.H. Ho, P.A. Heng, Reconstruction of volumetric ultrasound panorama based on improved 3D SIFT, Comput. Med. Imaging Graph. 33 (2009) 559–566, http://dx.doi.org/10.1016/j.compmedimag.2009.05.006.

[37] D. Ni, Y. Qu, X. Yang, Y.P. Chui, Volumetric ultrasound panorama based on 3D SIFT, Med. Image Comput. Comput. Assist. Interv. (2008) 52–60, http://dx.doi.org/10.1007/978-3-540-85990-1_7.

[38] D.G. Lowe, Distinctive image features from scale invariant keypoints, Int'l J. Comput. Vis. 60 (2) (2004) 91–110, http://dx.doi.org/10.1023/B:VISI.0000029664.99615.94.

[39] S.Y. Selmi, E. Promayon, J. Troccaz, 3D-2D ultrasound feature-based registration for navigated prostate biopsy: A feasibility study, in: 2016 38th Annu. Int. Conf. IEEE Eng. Med. Biol. Soc., 2016, pp. 4109–4112. http://dx.doi.org/10.1109/EMBC.2016.7591630.

[40] M. Baumann, P. Mozer, V. Daanen, J. Troccaz, Towards 3D Ultrasound Image Based Soft Tissue Tracking: A Transrectal Ultrasound Prostate Image Alignment System, in; Med. Image Comput. Comput. Interv., 2007, Part II., 2007, pp. 26–33. http://dx.doi.org/10.1007/978-3-540-75759-7_4.

[41] Z. Wang, G. Slabaugh, G. Unal, Tong Fang, Registration of ultrasound images using an information-theoretic feature detector. Zhe Wang New Jersey Institute of Technology Department of Electrical and Computer Engineering Newark, NJ 07102S Corporate Research Intelligent Vision and Reasoning D, (n.d.).

[42] Z. Wang, S. Member, G. Slabaugh, G. Unal, A.R. Case, An Information-Theoretic Detector Based Scheme for Registration of Speckled Medical Images, vol. 2 (n.d.).

[43] S. Golemati, A. Gastounioti, Ultrasound-image-based cardiovascular tissue motion estimation, IEEE Rev. Biomed. Eng. 9 (2016) 208–218, http://dx.doi.org/10.1109/RBME.2016.2558147.

[44] M. Alessandrini, B. Heyde, S. Queirós, S. Cygan, M. Zontak, O. Somphone, O. Bernard, M. Sermesant, H. Delingette, D. Barbosa, M. De Craene, M.O. Donnell, J. D'hooge, Detailed evaluation of five 3D speckle tracking algorithms using synthetic echocardiographic recordings, IEEE Trans. Med. Imaging 35 (2016) 1915–1926, http://dx.doi.org/10.1109/TMI.2016.2537848.

[45] P. Viola, W.M.I. Wells, Alignment by maximization of mutual information, Proc. IEEE Int. Conf. Comput. Vis. 24 (1995) 16–23, http://dx.doi.org/10.1109/ICCV.1995.466930.
[46] F. Maes, A. Collignon, D. Vandermeulen, G. Marchal, P. Suetens, Multimodality image registration by maximization of mutual information, IEEE Trans. Med. Imaging 16 (1997) 187–198, http://dx.doi.org/10.1109/42.563664.
[47] R. Shekhar, V. Zagrodsky, Mutual information-based rigid and nonrigid registration of ultrasound volumes, IEEE Trans. Med. Imaging 21 (2002) 9–22, http://dx.doi.org/10.1109/42.981230.
[48] C.R. Meyer, J.L. Boes, B. Kim, P.H. Bland, G.L. Lecarpentier, J.B. Fowlkes, M.A. Roubidoux, P.L. Carson, Semiautomatic registration of volumetric ultrasound scans, Ultrasound Med. Biol. 25 (1999) 339–347, http://dx.doi.org/10.1016/S0301-5629(98)00148-3.
[49] M.M.J. Letteboer, P.W.A. Willems, M.A. Viergever, W.J. Niessen, Non-rigid registration of 3D ultrasound images of brain tumours acquired during neurosurgery, in: Med. Image Comput. Comput. Assist. Interv. I, 2003, pp. 408–415.
[50] G. Narayanasamy, G.L. LeCarpentier, S. Zabuawala, J.B. Fowlkes, M. Roubidoux, S. Sinha, P.L. Carson, Non-rigid registration of three-dimensional (3D) grayscale and Doppler ultrasound breast images, in: Annu. Int. Conf. IEEE Eng. Med. Biol. – Proc., 2007, pp. 91–94. http://dx.doi.org/10.1109/IEMBS.2007.4352230.
[51] V. V. Karnik, A. Fenster, J. Bax, L. Gardi, I. Gyacskov, J. Montreuil, C. Romagnoli, A.D. Ward, Evaluation of inter-session 3D-TRUS to 3D-TRUS image registration for repeat prostate biopsies, in: Lect. Notes Comput. Sci. (Including Subser. Lect. Notes Artif. Intell. Lect. Notes Bioinformatics). 6362 LNCS, 2010, pp. 17–25. http://dx.doi.org/10.1007/978-3-642-15745-5_3.
[52] N.D. Nanayakkara, B. Chiu, A. Samani, J.D. Spence, G. Parraga, J. Samarabandu, A. Fenster, Nonrigid registration of carotid ultrasound and MR images using a "twisting and bending" model, Proc. SPIE 6914 (2008), http://dx.doi.org/10.1117/12.770337. 691411-691411-8.
[53] Z. Sun, H. Bai, B. Liu, Rigid and elastic registration for coronary artery IVUS images, Technol. Health Care 24 (2016) S455–S463, http://dx.doi.org/10.3233/THC-161168.
[54] G. Xiao, J.M. Brady, J.A. Noble, M. Burcher, R. English, Nonrigid registration of 3-D free-hand ultrasound images of the breast, IEEE Trans. Med. Imaging 21 (2002) 405–412, http://dx.doi.org/10.1109/TMI.2002.1000264.
[55] O.K. Øye, W. Wein, D.M. Ulvang, K. Matre, I. Viola, Real time image-based tracking of 4D ultrasound data, Med. Image Comput. Comput. Assist. Interv. 15 (2012) 447–454. http://www.ncbi.nlm.nih.gov/pubmed/23285582.
[56] B. Heyde, D. Barbosa, P. Claus, F. Maes, J. D'hooge, Influence of the grid topology of free-form deformation models on the performance of 3D strain estimation in echocardiography, in: Lect. Notes Comput. Sci. (Including Subser. Lect. Notes Artif. Intell. Lect. Notes Bioinformatics). 7945 LNCS, 2013, pp. 308–315. http://dx.doi.org/10.1007/978-3-642-38899-6_37.
[57] B. Heyde, R. Jasaityte, D. Barbosa, V. Robesyn, S. Bouchez, P. Wouters, F. Maes, P. Claus, J. D'hooge, Elastic image registration verses speckle tracking for 2-D myocardial motion estimation: a direct comparison in vivo, IEEE Trans. Med. Imaging 32 (2013) 449–459, http://dx.doi.org/10.1109/TMI.2012.2230114.
[58] B. Heyde, D. Barbosa, P. Claus, F. Maes, J. D'hooge, Three-dimensional cardiac motion estimation based on non-rigid image registration using a novel transformation model adapted to the heart, Stat. Atlases Comput. Model. Heart 7746 (2013) 142–150.
[59] M. Alessandrini, B. Heyde, S. Cygan, M. Sermesant, H. Delingette, O. Bernard, M. De Craene, J. D'Hooge, Elastic registration vs. block matching for quantification of cardiac function with 3D ultrasound: Initial results of a direct comparison in silico based on a new evaluation pipeline, in: IEEE Int. Ultrason. Symp. IUS, 2014, pp. 608–611. http://dx.doi.org/10.1109/ULTSYM.2014.0149.
[60] H. De Veene, P.B. Bertrand, N. Popovic, P.M. Vandervoort, P. Claus, M. De Beule, B. Heyde, Automatic mitral annulus tracking in volumetric ultrasound using non-rigid image registration, in: Proc. Annu. Int. Conf. IEEE Eng. Med. Biol. Soc. EMBS. 2015–Novem 2015, 1985–1988. http://dx.doi.org/10.1109/EMBC.2015.7318774.
[61] D. Zikic, W. Wein, A. Khamene, D.-A. Clevert, N. Navab, Fast deformable registration of 3D-ultrasound data using a variational approach, Med. Image Comput. Comput. Assist. Interv. 9 (2006) 915–923. http://far.in.tum.de/pub/zikic2006fast/zikic2006fast.pdf.
[62] R.E.E.S. Hefny, Wavelet-Based Variational Deformable Registration for Ultrasound Mohamed, 2010, pp. 1017–1020.
[63] M. Ledesma-Carbayo, J. Kybic, M. Desco, A. Santos, M. Suhling, P. Hunziker, M. Unser, Spatio-temporal nonrigid registration for ultrasound cardiac motion estimation, IEEE Trans. Med. Imaging 24 (2005) 1113–1126.
[64] T. Klein, M. Hansson, A. Karamalis, N. Navab, Registration of RF Ultrasound Data Using Hybrid Local Binary Patterns Computer Aided Medical Procedures (CAMP), Technische Universit at Malmö University, School of Technology, Sweden, 2012, pp. 1072–1075.
[65] P. Foroughi, P. Abolmaesumi, A modified HAMMER algorithm for deformable registration of ultrasound images, Int. Congr. Ser. 1281 (2005) 236–241, http://dx.doi.org/10.1016/j.ics.2005.03.201.
[66] D. Shen, C. Davatzikos, HAMMER: hierarchical attribute matching mechanism for elastic registration, IEEE Trans. Med. Imaging 21 (2002) 1421–1439, http://dx.doi.org/10.1109/TMI.2002.803111.
[67] S. Vijayan, S. Klein, E. Fagertun, F. Lindseth, B. Ystgaard, Validation of A Non-rigid Registration Method for Motion Compensation in 4D Ultrasound of the Liver, Norwegian University of Science and Technology, Trondheim, Norway SINTEF, Norway Biomedical Imaging Group Rotter, Dept. Medical Technology, 2013, pp. 780–783.
[68] K.K. Bhatia, J. Hajnal, A. Hammers, D. Rueckert, Similarity metrics for groupwise non-rigid registration, Med. Image Comput. Comput. Assist. Interv. 10 (2007) 544–552, http://dx.doi.org/10.1007/978-3-540-75759-7_66.
[69] C.T. Metz, S. Klein, M. Schaap, T. van Walsum, W.J. Niessen, Nonrigid registration of dynamic medical imaging data using nD+t B-splines and a groupwise optimization approach, Med. Image Anal. 15 (2011) 238–249, http://dx.doi.org/10.1016/j.media.2010.10.003.
[70] P. Foroughi, P. Abolmaesumi, Elastic registration of 3D ultrasound images, Med. Image Comput. Comput. Interv. (2005) 83–90.
[71] B.K.P. Horn, Closed-form solution of absolute orientation using unit quaternions, J. Opt. Soc. Am. A 4 (1987) 629, http://dx.doi.org/10.1364/JOSAA.4.000629.
[72] B.J.A. Nelder, R. Mead, A simplex method for function minimization, Comput. J. 7 (1964) 308–313, http://dx.doi.org/10.1093/comjnl/7.4.308.
[73] V. Lempitsky, C. Rother, S. Roth, A. Blake, Fusion Moves for Markov Random Field Optimization, vol. 32, 2009, pp. 1–15.
[74] D. Rueckert, L.I. Sonoda, C. Hayes, D.L. Hill, M.O. Leach, D.J. Hawkes, Nonrigid registration using free-form deformations: application to breast MR images, IEEE Trans. Med. Imaging 18 (1999) 712–721, http://dx.doi.org/10.1109/42.796284.
[75] D.W. Marquardt, An algorithm for least-squares estimation of nonlinear parameters, J. Soc. Ind. Appl. Math. 11 (1963) 431–441, http://dx.doi.org/10.1137/0111030.
[76] C. Zhu, R.H. Byrd, P. Lu, J. Nocedal, Algorithm 778: L-BFGS-B: Fortran subroutines for large-scale bound-constrained optimization, ACM Trans. Math. Softw. 23 (1997) 550–560, http://dx.doi.org/10.1145/279232.279236.
[77] M.J.D. Powell, On search directions for minimization algorithms, Math. Program. 4 (1973) 193–201, http://dx.doi.org/10.1007/BF01584660.
[78] J. Frednck Cornhill Shekhar, V. Zagrodsky, R. Shekhar, Mutual Information Based Registration of Cardiac Ultrasound Volumes, vol. XX, Ponsen & Looijen, 2000, pp. 1–21.
[79] M.J.D. Powell, An efficient method for finding the minimum of a function of several variables without calculating derivatives, Comput. J. 7 (1964) 155–162, http://dx.doi.org/10.1093/comjnl/7.2.155.
[80] H.W. Sorenson, Least-squares estimation: from Gauss to Kalman, IEEE Spectr. 7 (1970) 63–68, http://dx.doi.org/10.1109/MSPEC.1970.5213471.
[81] M.C. Yip, D.G. Lowe, S.E. Salcudean, R.N. Rohling, C.Y. Nguan, Tissue tracking and registration for image-guided surgery, IEEE Trans. Med. Imaging 31 (2012) 2169–2182, http://dx.doi.org/10.1109/TMI.2012.2212718.
[82] M.A. Fischler, R.C. Bolles, Random sample consensus: a paradigm for model fitting with applications to image analysis and automated cartography, Commun. ACM 24 (1981) 381–395.
[83] E. Haber, J. Modersitzki, Numerical methods for volume preserving image registration, Inverse Probl. 20 (2004) 1621–1638, http://dx.doi.org/10.1088/0266-5611/20/5/018.
[84] C.R. Meyer, J.L. Boes, B. Kim, P.H. Bland, K.R. Zasadny, P.V. Kison, K. Koral, K.A. Frey, R.L. Wahl, Demonstration of accuracy and clinical versatility of mutual information for automatic multimodality image fusion using affine and thin-plate spline warped geometric deformations, Med Image Anal. 1 (1997) 195–206, http://dx.doi.org/10.1016/S1361-8415(97)85010-4.
[85] Y. Liu, H.D. Cheng, J. Huang, Y. Zhang, X. Tang, J. Tian, An effective non-rigid registration approach for ultrasound image based on "demons" algorithm, J. Digit. Imaging 26 (2013) 521–529, http://dx.doi.org/10.1007/s10278-012-9532-0.
[86] S. Klein, M. Staring, J.P.W. Pluim, Evaluation of optimization methods for nonrigid medical image registration using mutual information and B-splines, IEEE Trans. Image Process. 16 (2007) 2879–2890, http://dx.doi.org/10.1109/TIP.2007.909412.
[87] S. Klein, J.P.W. Pluim, M. Staring, M.A. Viergever, Adaptive stochastic gradient descent optimisation for image registration, Int. J. Comput. Vis. 81 (2009) 227–239, http://dx.doi.org/10.1007/s11263-008-0168-y.
[88] S. Klein, M. Staring, M.A. Viergever, J. Pluim, Elastix: a toolbox for intensity-based medical image registration, IEEE Trans. Med. Imaging 29 (2010) 196–205, http://dx.doi.org/10.1109/TMI.2009.2035616.
[89] M.B.-N. and C. Gramkow, Fast Fluid Registration of Medical Images, in: Statew. Agric. L. Use Baseline 2015, vol. 1, 2015. http://dx.doi.org/10.1017/CBO9781107415324.004.
[90] F.L. Bookstein, Principal warps: thin-plate splines and the decomposition of deformations, IEEE Trans. Pattern Anal. Mach. Intell. 11 (1989) 567–585, http://dx.doi.org/10.1109/34.24792.
[91] S. Ourselin, A. Roche, G. Subsol, X. Pennec, N. Ayache, Reconstructing a 3D structure from serial histological sections, Image Vis. Comput. 19 (2001) 25–31, http://dx.doi.org/10.1016/S0262-8856(00)00052-4.
[92] X. Yang, H. Akbari, L. Halig, B. Fei, 3D non-rigid registration using surface and local salient features for transrectal ultrasound image-guided prostate biopsy, Proc. SPIE 7964 (2011) 79642V, http://dx.doi.org/10.1117/12.878153.
[93] X. Yang, B. Fei, 3D prostate segmentation of ultrasound images combining longitudinal image registration and machine learning, Proc. SPIE 8316 (2012) 831620, http://dx.doi.org/10.1117/12.912188.
[94] J. Kybic, M. Unser, Fast parametric elastic image registration, IEEE Trans. Image Process. 12 (2003) 1427–1442, http://dx.doi.org/10.1109/TIP.2003.813139.

[95] P. Besl, N. McKay, A method for registration of 3-D shapes, IEEE Trans. Pattern Anal. Mach. Intell. 14 (1992) 239–256, http://dx.doi.org/10.1109/34.121791.
[96] J. Banerjee, C. Klink, E.D. Peters, W.J. Niessen, A. Moelker, T. Van Walsum, 4D liver ultrasound registration, in: Lect. Notes Comput. Sci. (Including Subser. Lect. Notes Artif. Intell. Lect. Notes Bioinformatics). 8545 LNCS, 2014, pp. 194–202. http://dx.doi.org/10.1007/978-3-319-08554-8_20.
[97] H. Chui, A. Rangarajan, A new point matching algorithm for non-rigid registration, Comput. Vis. Image Underst. 89 (2003) 114–141, http://dx.doi.org/10.1016/S1077-3142(03)00009-2.
[98] C. Wachinger, R. Shams, N. Navab, Estimation of acoustic impedance from multiple ultrasound images with application to spatial compounding, in: IEEE Comput. Soc. Conf. Comput. Vis. Pattern Recognit. Work. CVPR Work, 2008. http://dx.doi.org/10.1109/CVPRW.2008.4563028.
[99] T.S. Yoo, The insight toolkit: An open-source initiative in data segmentation and registration, in: Vis. Handb., 2005, pp. 733–748. http://dx.doi.org/10.1016/B978-012387582-2/50039-3.
[100] S.Y. Sun, M. Gilbertson, B.W. Anthony, Probe localization for freehand 3D ultrasound by tracking skin features, in: Lect. Notes Comput. Sci. (Including Subser. Lect. Notes Artif. Intell. Lect. Notes Bioinformatics). 8674 LNCS, 2014, pp. 365–372. http://dx.doi.org/10.1007/978-3-319-10470-6_46.
[101] H. Rafii-Tari, P. Abolmaesumi, R. Rohling, Panorama ultrasound for guiding epidural anesthesia: A feasibility study, in: Lect. Notes Comput. Sci. (Including Subser. Lect. Notes Artif. Intell. Lect. Notes Bioinformatics). 6689 LNCS, 2011, pp. 179–189. http://dx.doi.org/10.1007/978-3-642-21504-9_17.
[102] H.A.D. Ashab, V.A. Lessoway, S. Khallaghi, A. Cheng, R. Rohling, P. Abolmaesumi, AREA: An augmented reality system for epidural anaesthesia, Proc. Annu. Int. Conf. IEEE Eng. Med. Biol. Soc. EMBS, 2012, pp. 2659–2663. http://dx.doi.org/10.1109/EMBC.2012.6346511.
[103] K. Rajpoot, V. Grau, J. Alison Noble, H. Becher, C. Szmigielski, The evaluation of single-view and multi-view fusion 3D echocardiography using image-driven segmentation and tracking, Med. Image Anal. 15 (2011) 514–528, http://dx.doi.org/10.1016/j.media.2011.02.007.